A new relaxation scheme for solving EHL problems

(E. Nurgat and M. Berzins)[a]

[a]School of Computer Studies, University of Leeds,
Leeds LS2 9JT, United Kingdom

A New Relaxation Scheme (NRS) is presented in this paper to solve Elasto Hydrodynamic Lubrication (EHL) point contact problems. The solutions obtained are compared with those obtained by Ehret [6] who employed the Distributive Relaxation Scheme (DRS) of Venner [2]. Results obtained using the two schemes are in close agreement which is very encouraging although it is too early to draw any conclusions. The new relaxation scheme thus provides an alternative approach to the distributive relaxation scheme.

1. INTRODUCTION

Over the last few decades various numerical algorithms have been presented for solving Elasto Hydrodynamic Lubrication (EHL) [1] point contact problems. One of the most effective method to date for solving these problems is the use of multigrid methods. Extensive use of multigrid methods in solving EHL problems have been presented by Venner [2] and [3] and Venner and Lubrecht [4]. The development of multigrid multi-integration by Brandt and Lubrecht [5] and Venner [2] has also greatly enhanced the efficiency of multigrid methods for EHL problems. Venner [2] and more recently Ehret [6] employed Gauss-Seidel line and Jacobi distributive line relaxation schemes with multigrid multi-integration scheme to solve EHL problems. This scheme is known as the Distributive Relaxation Scheme (DRS).

The aim of this paper is to present a New Relaxation Scheme (NRS) to solve EHL point contact problems using the multigrid method. The new relaxation scheme employs Gauss-Seidel and Jacobi line relaxation schemes and is an alternative approach to the distributive relaxation scheme. In both the distributive relaxation scheme of Venner [2] and the new relaxation scheme, the choice of the relaxation scheme is dependent on the value of the coefficient ϵ of the Reynolds equation. The main difference between these two approaches is in how they treat the contact region of the EHL problem. Various test problems are used in order to compare the results obtained using the distributive relaxation scheme employed by Ehret [6] and the new relaxation scheme.

The layout of the rest of the paper is as follows. In section (2) we introduce the form of the equations to be solved. The multigrid method to be used is described in section (3) while section (4) describes different relaxation schemes which includes the distributive and the new relaxation schemes. Section (5) describes the test problems to be used in the comparison between the two relaxation schemes and the paper is concluded in section (6).

2. GOVERNING EQUATIONS

The mathematical model describing the isothermal EHL circular contact problem with oil entrainment in the positive X-direction consists of three non-dimensional equations. The Reynolds Equation relates pressure (P) to the film thickness (H) for a lubricant characterised by a pressure dependent viscosity η and density ρ

$$L(P) = \frac{\partial}{\partial X}\left(\epsilon \frac{\partial P}{\partial X}\right) + \frac{\partial}{\partial Y}\left(\epsilon \frac{\partial P}{\partial Y}\right)$$

$$-\frac{\partial (\rho H)}{\partial X} = 0\ ,\ X, Y \in [X_a, X_b] \times [Y_a, Y_b] \qquad (1)$$

with the cavitation condition $P \geq 0$ and the boundary condition $P = 0$. The non-dimensionalisation is expressed in terms of the so-called Moes parameters L and M, [7]. Pressure

is in units of the maximum Hertzian pressure

$$p_h = \frac{L}{\alpha\pi}\sqrt[3]{\frac{3M}{2}} \tag{2}$$

where α is the pressure coefficient of viscosity of the lubricant. X and Y are in units of Hertzian radius (b). Film thickness is in units of b^2/R, where R is the reduced radius of the contact. ϵ is given by:

$$\epsilon = \frac{\rho H^3}{\eta\lambda} \tag{3}$$

where $\rho = 1 + \frac{\mu p_h P}{1+v p_h P}$ if $P > 0$, otherwise $\rho = 1$ ($\mu = 5.8 \times 10^{-10}$ and $v = 1.68 \times 10^{-9}$, [8]) , $\eta = \exp\{\frac{\alpha p_0}{z}[-1 + (1 + \frac{p_h}{p_0}P)^z]\}$ ($p_0 = 1.98\times10^8$ and $z = 0.68$, [9]) and $\lambda = \frac{4\pi}{M}\sqrt[3]{\frac{2}{3M}}$.

The Film Thickness Equation, $H(X,Y)$, computes the elastic distortion of the surfaces caused by the pressure in the film and is written as:

$$H(X,Y) = H_0 + \tfrac{X^2}{2} + \tfrac{Y^2}{2} + \frac{2}{\pi^2}\int_{Y_a}^{Y_b}\int_{X_a}^{X_b}\frac{P(X',Y')\,dX'\,dY'}{\sqrt{(X-X')^2+(Y-Y')^2}} \tag{4}$$

where H_0 is a constant.

The final equation is the Force Balance Equation which ensures that the integral over the pressure balances the external applied load:

$$\int_{Y_a}^{Y_b}\int_{X_a}^{X_b} P(X,Y)\,dX\,dY = \frac{2\pi}{3}. \tag{5}$$

2.1. Finite difference discretisation of governing equations

The governing equations are discretised with the direction of flow in the X-direction and mesh spacings h_x and h_y in the X and Y directions respectively. Due to symmetry, only half the domain is used in the Y-direction. Reynolds Equation (1) is discretised at each non boundary mesh point (i,j), $((i-1)h_x + X_a, (j-1)h_y + Y_a)$ where $X, Y \in [X_a, X_b]\times[Y_a, Y_b]$, using central and backward differencing to get:

$$L_{i,j} = \epsilon_{i-\frac{1}{2},j}(P_{i-1,j} - P_{i,j}) + \epsilon_{i+\frac{1}{2},j}(P_{i+1,j} - P_{i,j}) + h_x^2 h_y^{-2}(\epsilon_{i,j-\frac{1}{2}}(P_{i,j-1} - P_{i,j}) + \epsilon_{i,j+\frac{1}{2}}(P_{i,j+1} - P_{i,j})) - h_x(\rho_{i,j}H_{i,j} - \rho_{i-1,j}H_{i-1,j}) \tag{6}$$

where, $\epsilon_{i+\frac{1}{2},j}, \epsilon_{i-\frac{1}{2},j}, \epsilon_{i,j+\frac{1}{2}}$ and $\epsilon_{i,j-\frac{1}{2}}$ ($i = 2,\ldots,m_x-1$; $j = 2,\ldots,n_y-1$) denote the values of ϵ at the intermediate locations midway between mesh points. m_x and n_y are the maximum number of points in X and Y directions respectively.

The discretised film thickness equation (4) at a point (i,j) is given by:

$$H_{i,j} = H_0 + \frac{X_i^2}{2} + \frac{Y_j^2}{2} + d_{i,j} \tag{7}$$

where H_0 is a constant and $d_{i,j}$ is the elastic deformation of the material due to the applied load. The elastic deformation of the surface is derived by dividing the pressure distribution into rectangular blocks of uniform pressure. Thus the elastic deformation, $d_{X,Y}$, at a point (X,Y) due to the uniform pressure over the rectangular area $2a2b$ is given by Venner [2]

$$d_{X,Y} = \frac{2P}{\pi^2}\int_{-b}^{b}\int_{-a}^{a}\frac{dX'\,dY'}{r} \tag{8}$$

where $r = \sqrt{(X-X')^2 + (Y-Y')^2}$.

If the entire domain is divided into equal rectangular areas, then from Dowson and Hamrock [10], the elastic deformation, $d_{i,j}$, at a point (i,j) due to contributions of all rectangular areas of uniform pressure is given by:

$$d_{i,j} = \frac{2}{\pi^2}\sum_{k=1}^{m_x}\sum_{l=1}^{n_y} K_{m,n}P_{k,l} \tag{9}$$

where, $m = |i-k|+1$, $n = |j-l|+1$, m_x and n_y are the maximum number of points in the X and Y directions respectively. The coefficients $K_{m,n}$ are independent of pressure, P.

One advantage of a regular mesh is that the $m_x n_y$ coefficients need only be calculated once and stored. In contrast, on an irregular mesh it is necessary to store $m_x n_y$ coefficients for each mesh point.

The force balance equation (5) determines the value of the integration constant H_0 and is discretised as follows:

$$h_x h_y \sum_{i=1}^{m_x}\sum_{j=1}^{n_y} P_{i,j} - \frac{2\pi}{3} = 0. \tag{10}$$

3. MULTIGRID METHOD

The use of multigrid methods in solving EHL problems was introduced by Lubrecht [11], who through his extensive work has made the multigrid method an important technique in solving such problems. The use of multigrids for solving EHL line and point contact problems has been described by Venner [2].

The concept of multigrid iteration depends on the asymptotic nature of errors associated with iterative schemes and how the schemes reduce these errors. Smooth error components associated with low frequencies are hardly reduced with the classical iterative schemes, thus resulting in slow convergence. The opposite is true for error components with wavelength of the order of the mesh spacing. However, low frequency error components can be adequately represented on coarser grid. In a multilevel solver, which makes use of a series of coarser grids, each error component is reduced until it becomes smooth when the same procedure is applied on a coarser grid.

The FDMG Multigrid Software of Shaw [12] is used as a starting point for implementing the multigrid technique. FDMG employs the Multigrid Full Approximation Scheme (FAS) to solve nonlinear systems of partial differential equations using either V or W coarse grid correction cycles. The Jacobi or Gauss Seidel iterative method can be used as a smoother. The option for the type of restriction is either injection or full weighting [7].

EHL problems are nonlinear. Thus, when using multigrids, the standard Correction Scheme can not be used and the Full Approximation Scheme must be used instead. In the cavitation region, in which negative pressures may be computed by the solver, the Reynolds equation is not valid and the computed negative pressures are set to zero in the standard manner as used by Venner [2]. The cavitation region is treated with the multigrid method by using injection near and in the cavitational region when transferring the residual to the coarse grid. Full weighting is used in the remaining part of the domain. The elastic deformation and force balance equations get updated on each grid using the updated pressure values. The only substantial modification to FDMG has been to take symmetry boundary conditions and cavitation into consideration.

The solution for the isothermal point contact problem is obtained by making use of strong coupling in the direction of flow, the X-direction. Thus the discrete equations are solved simultaneously on a line of points, sweeping across the grid only in the positive Y-direction due to symmetry. On each line of points, the new relaxation scheme is employed, as described in section (4.3).

4. RELAXATION SCHEMES

The coefficient ϵ of the Reynolds equation (1) varies several orders of magnitude over the calculational domain. In both the inlet and outlet regions $\epsilon >> 1$ whereas in the contact region ϵ is very close to zero. Hence, in the dry contact region, i.e. $(X^2 + Y^2) \leq 1$, the integral aspect of the problem dominates whereas in the remaining part of the domain the problem behaves like a differential problem. When ϵ is small Reynolds equation (1) reduces to $\frac{\partial (\rho H)}{\partial X} = 0$ which is a relation in the X-direction only. Consequently when discretised there is no direct coupling via pressure between adjacent grid points in Y-direction. When ϵ is large the term $\frac{\partial (\rho H)}{\partial X}$ in Reynolds equation (1) is small compared to the differential terms. Thus the Reynolds equation (1) has the form of the 2-D Poisson type equation. The value of ϵ plays an important role in deciding which relaxation process to apply to the solution of the discretised Reynolds equation (6) with $H_{i,j}$ evaluated using equation (7). The relaxation process employed must be a stable error smoother over the entire domain and must be able to cope with the extreme values of ϵ which are a nonlinear function of pressure. The general approach taken in the successful distributive relaxation scheme of Venner [2] (see also Ehret [6]) and also in the new relaxation scheme described here is to make the choice of relaxation scheme dependent on the value of ϵ. The precise difference between the schemes will be described in section (4.4).

When ϵ is large, (a Poisson type problem), a one point Gauss-Seidel relaxation provides good error smoothing and stability. This is where given an approximation $\tilde{P}_{i,j}$ and the associated approx-

imation $\tilde{H}_{i,j}$ to $P_{i,j}$ and $H_{i,j}$ respectively, a new approximation $\overline{P}_{i,j}$ is computed using

$$\overline{P}_{i,j} = \tilde{P}_{i,j} + \left(\frac{\partial \tilde{L}_{i,j}}{\partial \tilde{P}_{i,j}} \right)^{-1} r_{i,j} \tag{11}$$

where $r_{i,j}$ is the residual at the point (i,j) and $\tilde{L}_{i,j} = L(\tilde{P}_{i,j})$ is given by equation (6). However, the performance of a one point Gauss-Seidel relaxation begins to deteriorate as ϵ decreases. Firstly the relaxation becomes unstable - low frequency error components are amplified and the relaxation process diverges. Secondly, due to the loss of coupling in the Y-direction, the relaxation becomes ineffective in reducing high frequency error components in Y-direction.

The problem of stability can be overcome by using a relaxation scheme which has properties of both Gauss-Seidel and Jacobi relaxations. For a standard Gauss-Seidel relaxation the new updated solution get used immediately in relaxing subsequent equations whereas for a standard Jacobi relaxation the new updated solution replaces the old one at the end of a complete sweep. The relaxation scheme used in order to achieve stability depends very much on the value of ϵ which is much smaller in the contact region than the non-contact region of the computational domain.

The problem of loss of coupling can be overcome by making use of line relaxation instead of point relaxation. This implies that instead of visiting the grid points one by one in some order, e.g. lexicographic order, and solving the discrete equation at each grid point, a system of discrete equations on a line of points are solved simultaneously. This must be done on a line which is in the direction of strong coupling. For EHL point contact problems there is strong coupling in the X-direction. Hence, we use points on a line in the X-direction, known as I-Line relaxation. That is on a line $Y = j$ $(j = 1, \ldots, n_y)$, where n_y is the maximum number of points in the Y-direction.

4.1. I-Line relaxation

Suppose $\underline{\tilde{P}}$ is an approximation to the true solution $\underline{P}$ then at a point (i,j), $\tilde{L}_{i,j} = L(\underline{\tilde{P}})_{i,j} \neq 0$ and $L_{i,j} = L(\underline{P})_{i,j} = 0$. Taylors theorem gives:

$$L_{i,j} = \tilde{L}_{i,j} + \sum_{l=1}^{n_y} \sum_{k=1}^{m_x} \frac{\partial \tilde{L}_{i,j}}{\partial \tilde{P}_{k,l}} \Delta P_{k,l} + O(\Delta P)^2 \tag{12}$$

where $\tilde{L}_{i,j} = L(\tilde{P}_{i,j})$ is the discretised Reynolds equation (6) at the point (X_i, Y_j). If we only consider points at $(i-1,j)$, (i,j) and $(i+1,j)$ then equation (12) can be rewritten as:

$$\begin{aligned} &\frac{\partial \tilde{L}_{i,j}}{\partial \tilde{P}_{i-1,j}} \Delta P_{i-1,j} + \frac{\partial \tilde{L}_{i,j}}{\partial \tilde{P}_{i,j}} \Delta P_{i,j} \\ &+ \frac{\partial \tilde{L}_{i,j}}{\partial \tilde{P}_{i+1,j}} \Delta P_{i+1,j} + \tilde{L}_{i,j} = 0 \,. \end{aligned} \tag{13}$$

For a constant j, that is on a line $Y = j$, equation (13) results in a tridiagonal system of equations which are solved simultaneously for the correction term $\Delta \underline{P}$. Having obtained $\Delta \underline{P}$, a new approximation $\overline{P}_{i,j}$ to $\tilde{P}_{i,j}$ is computed using:

$$\overline{P}_{i,j} = \tilde{P}_{i,j} - W \Delta P_{i,j} \tag{14}$$

where W is a damping factor. A correct choice of W is critical to ensure convergence of the method.

4.2. Distributive relaxation scheme

The distributive relaxation scheme works on the principle that the relaxation process remains local. That is relaxing at a point X_i has minimal effect at points X_j far away from X_i.

The distributive relaxation scheme employed by both Venner [2] and Ehret [6] makes use of Jacobi Distributive Line Relaxation (JDLR), Gauss-Seidel Line Relaxation (GSLR) and Point Gauss-Seidel (PGS) depending on the pressure values on the domain. JDLR is employed in regions of domain where pressure is large, which means ϵ is small, whereas in the remaining part of the domain, excluding the cavitation region where PGS is employed, GSLR is employed. Gauss-Seidel line relaxation and point Gauss-Seidel schemes employed are as described in section (4).

When using JDLR a new approximation $\overline{P}_{i,j}$ to $\tilde{P}_{i,j}$ is computed using

$$\overline{P}_{i,j} = \tilde{P}_{i,j} + \delta P_{i,j} \tag{15}$$

where $\delta P_{i,j} = \Delta P_{i,j} - \frac{1}{4}(\Delta P_{i-1,j} + \Delta P_{i+1,j} + \Delta P_{i,j-1} + \Delta P_{i,j+1})$. A new approximation $\overline{H}_{i,j}$ to $\tilde{H}_{i,j}$ is also computed using

$$\overline{H}_{i,j} = \tilde{H}_{i,j} + \frac{2}{\pi^2} \sum_{k=i-1}^{i+1} \sum_{l=j-1}^{j+1} K_{i,k,j,l} \delta P_{k,l} \,. \quad (16)$$

It is not necessary to obtain the exact representation of $\overline{H}_{i,j}$ as is shown by Wang [13]. The correction terms, $\Delta \underline{P}$, are obtained using line relaxation by solving a system of equations of the form given by

$$\frac{\partial \tilde{L}_{i,j}}{\partial \tilde{P}_{i-2,j}} \Delta P_{i-2,j} + \frac{\partial \tilde{L}_{i,j}}{\partial \tilde{P}_{i-1,j}} \Delta P_{i-1,j} + \frac{\partial \tilde{L}_{i,j}}{\partial \tilde{P}_{i,j}} \Delta P_{i,j} + \frac{\partial \tilde{L}_{i,j}}{\partial \tilde{P}_{i+1,j}} \Delta P_{i+1,j} + \frac{\partial \tilde{L}_{i,j}}{\partial \tilde{P}_{i+2,j}} \Delta P_{i+2,j} + \tilde{L}_{i,j} = 0 \,. \quad (17)$$

Since JDLR is a Jacobi relaxation scheme, the solution $\underline{P}$ gets updated after a complete sweep. The numerical scheme employed makes use of the full multigrid solver and of the multi-integration techniques [2] and [5] to compute elastic deformation.

4.3. New relaxation scheme

The new relaxation scheme makes use of Jacobi and Gauss-Seidel line relaxation schemes depending on the value of the coefficient ϵ of the Reynolds equation (1). Jacobi and Gauss-Seidel line relaxation schemes are respectively employed in the contact and non-contact regions of the computational domain. This new relaxation scheme is employed in the following manner:

Having obtained $\Delta \underline{P}$ using I-Line relaxation on the line $Y = j$ and before applying I-Line relaxation on the line $Y = j + 1$, at every point on the line $Y = j$ which lies in the non-contact region, as shown in Figure (1), a new approximation $\overline{P}_{i,j}$ to $\tilde{P}_{i,j}$ is computed using equation (14) with the damping factor W lying in the range 0.5 to 0.8. Besides this, all the correction terms $\Delta \underline{P}$ in the contact region on the line $Y = j$ are saved in order to update the solution in the contact region after a complete sweep.

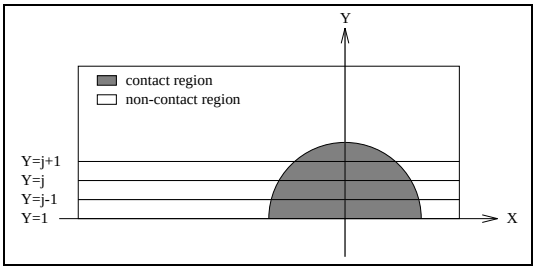

Figure 1 Representation of contact and non-contact regions.

After all interior lines j have been visited, that is after a complete sweep, a new approximation $\overline{P}_{i,j}$ to $\tilde{P}_{i,j}$ is computed at every point on the entire grid which lies only in the contact region using equation (14) but this time the damping factor W lies in the range 0.1 to 0.2. Thus the saved values of the corrections $\Delta \underline{P}$ for the portions of each of the lines in the contact region, shown as shaded region in Figure (1), are added en-masse at the end of the iteration. This corresponds to a block Jacobi method. Having updated all the pressure values on the entire grid, the elastic deformation at every point on the entire grid is recalculated using the new pressure values.

4.4. Differences between DRS and NRS

The Distributive Relaxation Scheme (DRS) differs from the New Relaxation Scheme (NRS) in many ways and it is now possible to describe the differences between these two relaxation schemes.

The DRS makes use of Jacobi distributive and Gauss-Seidel line relaxation schemes in the contact and non contact regions of the computational domain respectively whereas the NRS makes use of Jacobi and Gauss-Seidel line relaxation schemes in the contact and non contact regions of the computational domain respectively. Besides this, the DRS also makes use of the point Gauss-Seidel scheme in the cavitation region. In the DRS, regions of the domain where JDLR is employed, the correction terms at the points (i, j), $(i \pm 1, j)$ and $(i, j \pm 1)$ are used to

update the solution at the point (i, j) as shown in equation (15) whereas in the remaining part of the domain, where Gauss-Seidel line relaxation and point Gauss-Seidel schemes are employed, the method used to update solution is similar to the one used in the NRS. The solution, P, at a point (i, j) in the NRS is updated using the correction term $\Delta P_{i,j}$ as shown in equation (14). The correction terms in the NRS are obtained by solving a tridiagonal system of equations as can be seen from equation (13) whereas in the DRS, regions of domain where JDLR is employed, the system of equations are pentadiagonal as can be seen from equation (17). However, they will be tridiagonal in regions where the Gauss-Seidel line relaxation scheme is employed. In DRS a new film thickness equation (16) is used when dealing with the couette term of the Reynolds equation (1). This is not the case in the NRS.

The main difference between the DRS and the NRS is in the contact region of the computational domain. This is where the Jacobi distributive line relaxation scheme is employed by the DRS and the Jacobi line relaxation scheme is employed by the NRS. The system of equations solved in order to obtain the correction terms and the way pressures are updated at a point (i, j) are also different in the two schemes. The results obtained, as shown in section (5), show that the NRS appears to work as well as the DRS, though the NRS is a much simpler scheme than the DRS.

5. TEST PROBLEMS

Results obtained using Multigrid Multi-Integration method (MIM) [2], which employs distributive relaxation scheme, and Multigrid method (MM), which makes use of the new relaxation scheme are compared. Three test problems defined by the Moes parameters M and L are considered where for each test problem the Moes parameter L was fixed at 10, 14 and 28 while the Moes parameter M was varied from 10 to 200 for the three cases. A value of $\alpha = 2.2 \times 10^{-8}$, hence, the maximum Hertzian pressure varied from 0.44 GPa to 2.71 GPa, was considered in all the test problems.

Test problems solved using MIM employed 513×513 mesh points on the finest grid and 17×17 mesh points on the coarsest grid. When the Moes parameter L was fixed at 10 and 28, a finest grid of 129×129 and a coarsest grid of 17×17 was used when solved using MM. However, for the case $L = 14$, a finest grid with 257×257 mesh points was employed. Both MIM and MM make use of a full multigrid scheme and the discretisation schemes are the same for the two methods as described in section (2.1).

The minimum and central film thicknesses obtained using the two methods have been compared and the results are shown in Tables 1 and 2. The minimum and central film thicknesses obtained using the two methods are in general agreement especially for the case $L = 14$ where the computational domains employed by the two schemes are the same and the mesh resolution of the solutions obtained using the MM scheme is higher than that of the other two cases, L=10 and L=28. However, a discrepancy of about 5% is observed for the other two cases, L=10 and L=28. This can be attributed to the different size of domains employed by the two schemes and primarily to the differences in the mesh resolution. For solutions obtained using the MIM scheme, the domain employed was dependent on the Moes parameter M and the following domains were employed: $[M \leq 10 \Rightarrow -7 \leq X \leq 2 \text{ and } -4.5 \leq Y \leq 4.5]$, $[10 < M \leq 50 \Rightarrow -5 \leq X \leq 2 \text{ and } -3.5 \leq Y \leq 3.5]$ and $[50 < M \leq 500 \Rightarrow -4.5 \leq X \leq 1.5 \text{ and } -3 \leq Y \leq 3]$. For solutions obtained using the MM scheme, the above domain was employed only for the case $L = 14$. However, when the Moes parameter L was fixed at 10 and 28 the domain employed was $-4.5 \leq X \leq 1.5$ and $-3 \leq Y \leq 3$. Figure 2 shows the pressure profile for the case $L = 14$ and $M = 100$.

The efficiency of the solution is based on the Root Mean Square Residual (RMSR) and the mean absolute residual (Norm0). The solutions obtained by Ehret using MIM, Norm0 was of the order 1.0×10^{-7} and hardly any change in Norm0 was observed after a number of iterations. For the solutions obtained using MM, the RMSR and Norm0 were of the order 1.0×10^{-4} and 1.0×10^{-5} respectively. Hardly any change was also observed in the RMSR and Norm0 after about 5

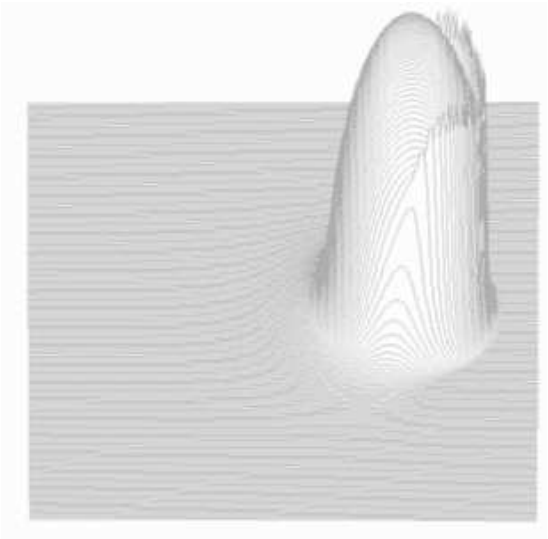

Figure 2 3D pressure profile for M=100 & L=14 on a 257×257 mesh with domain $[-4.5 \leq X \leq 1.5$ & $-3 \leq Y \leq 3]$.

to 6 multigrid iterations (V-cycles). An analysis of the residuals showed that the main reason in not achieving very small residuals was due to the free boundary in the cavitation region and the pressure spikes. Work is still being done in order to reduce residuals in these regions.

Results obtained by Ehret using MIM were carried out on a Sun Sparcstation 20 whereas an SGI R8000 was used for the solutions obtained using multigrid method which employed the new relaxation scheme. When using MIM, 5 V-cycles are performed in about 30 minutes whereas when MM is employed, time taken to do 5 V-cycles was about 60 minutes. The bulk of the difference in this computing time is due to the use of multi-integration method by Ehret. Adoption of this approach in the new relaxation scheme may well mean that the two procedures are more evenly matched computationally.

6. CONCLUSION

A new relaxation scheme for solving EHL problems have been presented in this paper and the numerical results obtained are compared with those obtained by Ehret [6] who employed distributive relaxation scheme. The results obtained show that the new relaxation scheme appears to work as well as the distributive relaxation scheme. This new relaxation scheme is very simple and the results obtained are very encouraging. However, it is too early to draw any conclusions at this stage as more work still needs to be done in order to analyse the accuracy of the solutions. An analysis of the residuals showed that in the free boundary cavitation and the pressure spike regions the residuals are relatively higher than those in the other regions of the computational domain. The results obtained also indicate that both the size of the computational domain and the mesh resolution does have an influence on the solutions.

7. ACKNOWLEDGEMENTS

The authors would like to thank EPSRC and Shell Research Ltd, Thornton Research Centre for funding this work through an EPSRC CASE Studentships for E.N. Our colleagues at Leeds in the Mechanical Engineering Department D. Dowson, C. Taylor and P. Ehret are thanked for providing much constructive advice and support. Gareth Shaw of NAG Ltd is thanked for supplying the FDMG code.

REFERENCES

1. R. Gohar, Elastohydrodynamics, Ellis Horwood Limited, Chichester, England, 1988.
2. C.H. Venner, Multilevel Solution of the EHL Line and Point Contact Problems, PhD. Thesis, University of Twente, The Netherlands, ISBN 90-9003974-0, 1991.
3. C.H. Venner, Higher-Order Multilevel Solvers for the EHL Line and Point Contact Problem, Journal of Tribology, Vol. 116 (1994) 741-750.
4. C.H. Venner and A.A. Lubrecht, Numerical Simulation of a Transverse Ridge in a Circular EHL Contact Under Rolling/Sliding, Journal of Tribology, Vol. 116 (1994) 751-761.
5. A. Brandt and A.A. Lubrecht, Multilevel Matrix Multiplication and Fast Solution of In-

Table 1 Minimum film thicknesses for $L = 10$, $L = 14$ and $L = 28.3$

	$L = 10.0$	$U = 0.089 \times 10^{-10}$	$G = 4869$	
M	W ($\times 10^{-6}$)	Ph(GPa)	MIM ($\times 10^{-6}$)	MM ($\times 10^{-6}$)
20	0.173	0.44	12.08	12.31
50	0.433	0.60	10.26	10.64
100	0.867	0.76	8.88	8.99
200	1.733	0.96	7.43	7.40
	$L = 14.0$	$U = 0.343 \times 10^{-10}$	$G = 4869$	
M	W ($\times 10^{-6}$)	Ph(GPa)	MIM ($\times 10^{-6}$)	MM ($\times 10^{-6}$)
20	0.477	0.62	28.98	28.55
50	1.191	0.85	25.02	25.28
100	2.384	1.07	21.87	21.82
200	4.767	1.35	18.73	18.71
	$L = 28.3$	$U = 5.707 \times 10^{-10}$	$G = 4869$	
M	W ($\times 10^{-6}$)	Ph(GPa)	MIM ($\times 10^{-6}$)	MM ($\times 10^{-6}$)
20	3.927	1.26	185.57	190.83
50	9.818	1.72	166.12	176.87
100	19.64	2.15	148.49	148.19
200	39.27	2.71	129.87	125.93

tegral Equations, Journal of Comp. Physics, No. 2 (1990) 348-370.

6. P. Ehret, D. Dowson, C.M. Taylor and D. Wang, Analysis of EHL Point Contacts with Multigrid Methods, To be Published in IMECHE, Part C.
7. A.A. Lubrecht, W.E. ten Napel and R. Bosma, Multigrid - An Alternative Method of Solution for Two-dimensional Elastohydrodynamically Lubricated Point Contact Calculations, ASME Journal of Tribology, Vol. 109 (1987) 437-443.
8. D. Dowson and G.P. Higginson, Elastohydrodynamic Lubrication, Pergamon Press, 1977.
9. C.J.A. Roelands, Correlational Aspects of the Viscosity- Temperature-Pressure Relationship of Lubricating Oils, PhD. Thesis, Technische Hogeschool Delft, Netherlands, 1966.
10. D. Dowson and B.J. Hamrock, Numerical Evaluation of the Surface Deformation of Elastic Solids Subjected to a Hertzian Contact Stress, ASLE Trans., Vol. 19 No. 4 (1976) 279-286.
11. A.A. Lubrecht, W.E. ten Napel and R. Bosma, Multigrid - An Alternative Method of Calculating Film Thickness and Pressure Profiles in Elastohydrodynamically Lubricated Line Contacts, ASME Journal of Tribology, Vol. 108 No. 4 (1986) 551-556.
12. G.J. Shaw, FDMG Multigrid Software Manual, version 3.0.

Table 2 Central film thicknesses for $L = 10$, $L = 14$ and $L = 28.3$

	$L = 10.0$	$U = 0.089 \times 10^{-10}$	$G = 4869$	
M	W ($\times 10^{-6}$)	Ph(GPa)	MIM ($\times 10^{-6}$)	MM ($\times 10^{-6}$)
20	0.173	0.44	17.79	18.27
50	0.433	0.60	17.17	18.02
100	0.867	0.76	16.59	17.24
200	1.733	0.96	15.66	16.59
	$L = 14.0$	$U = 0.343 \times 10^{-10}$	$G = 4869$	
M	W ($\times 10^{-6}$)	Ph(GPa)	MIM ($\times 10^{-6}$)	MM ($\times 10^{-6}$)
20	0.477	0.62	41.54	41.03
50	1.191	0.85	40.30	41.01
100	2.384	1.07	39.13	39.25
200	4.767	1.35	37.71	38.16
	$L = 28.3$	$U = 5.707 \times 10^{-10}$	$G = 4869$	
M	W ($\times 10^{-6}$)	Ph(GPa)	MIM ($\times 10^{-6}$)	MM ($\times 10^{-6}$)
20	3.927	1.26	247.82	252.94
50	9.818	1.72	245.02	255.99
100	19.64	2.15	239.56	245.61
200	39.27	2.71	233.76	241.44

13. D. Wang, Elastohydrodynamic Lubrication of Point Contacts for Layers of Soft Solids and for Monolithic Hard Materials in the Transient Bouncing Ball Problems, PhD. Thesis, Department of Mechanical Engineering, University of Leeds, 1994.